International Journal of Engineering and Geosciences
https://dergipark.org.tr/en/pub/ijeg
e-ISSN 2548-0960

Determination of the appropriate zone on dam surface for floating photovoltaic system installation using RS and GISc technologies

Osman Salih Yılmaz [*1], **Fatih Gülgen** [2], **Ali Murat Ateş** [3]

[1] *Manisa Celal Bayar University, Geographical Information Systems Department, Türkiye*
[2] *Yıldız Technical University, Geomatics Engineering Department, Türkiye*
[3] *Manisa Celal Bayar University, Computer and Instructional Technologies Department, Türkiye*

Keywords
Remote sensing
GIS
Google Earth Engine
Solar power plant
Solar analysis

Research Article
DOI: 10.26833/ijeg.1052556

Received: 02.01.2022
Accepted: 11.02.2022
Published: 13.04.2022

Abstract

This study aims to reveal suitable places where floating photovoltaic-solar power plants (FPV-SPPs) can be installed on the dam surface using the possibilities of remote sensing (RS) and geographical information science (GISc) technologies. Past satellite images from Landsat and Sentinel platforms allow researchers to analyse shoreline changes in the dam surface. Shoreline extraction is a crucial process for the FPV-SPP to stay afloat despite external constraints. In this study, changes in dam water levels were determined by classifying 20-year satellite images and analysing a 32-year global surface water dynamics dataset. The water surface area was calculated as 1,562.40 ha using the random forest (RF) algorithm and the normalized differences water index (NDWI) on Google Earth Engine (GEE) cloud platform. In addition, solar analysis was carried out with GISc using annual solar radiation maps shuttle radar topography mission (SRTM) data, which directly affects the energy production of FPV-SPPs. It has been calculated that the solar radiation on the water surface varies between 1,554 kWh/m^2-year and 1,875 kWh/m^2-year. These calculated values were divided into five different classes, and it was observed that 88.5% of the dam surface had a very high level of solar radiation compared to other areas. Higher efficiency will be obtained from the FPV-SPP to be installed in this region compared to the systems to be installed in other regions. It has been observed that the radiation values in other parts of the water surface are lower due to topographic shading. These analyses revealed energy zones with high production potential, thereby easing the decision-making process for investors planning to establish FPV-SPPs.

1. Introduction

Ensuring sustainability of water resources is very important in environmental, economic, and strategic terms for humans, animals, plants and the ecosystem [1]. One of the water resources is the dams that produce hydroelectric energy and at the same time are built to prevent floods in places with abundant rainfall [2]. The amount of water in dams changes frequently due to uses for agricultural irrigation, energy production activities, and climatic changes. Monitoring these changes is a necessity within the scope of understanding hydrological processes and good management of water resources [3]. Remote sensing technology, with its advantages of continually, rapidly, informatively and dynamically monitoring the large-scale environment, is one of the important tools in terms of obtaining information about the change in the dam coastal region [4, 5]. and tracking the water dynamics [6]. Changes in physically inaccessible regions can be quickly, cost-effectively, and advantageously monitored using medium-resolution optical images obtained from satellites, such as Landsat and Sentinel [7].

Rapid population growth and industrial investments exponentially increase countries' need for energy. Approximately 81% of the total energy consumption in the world is met by fossil fuel resources [8]. The intensive use of fossil fuels causes the emission of harmful gases and the deterioration of the natural balance. Renewable energy systems that transform natural resources into electrical energy stand out as alternatives to fossil fuels. Among these systems, solar power plants (SPPs)

* **Corresponding Author**
*(osmansalih.yilmaz@cbu.edu.tr) ORCID ID 0000 - 0003 - 4632 - 9349
(fgulgen@yildiz.edu.tr) ORCID ID 0000 - 0002 - 8754 - 9017
(murat.ates@cbu.edu.tr) ORCID ID 0000-0002-2815-1404

Cite this article
Yılmaz, O. S., Gülgen, F., & Ateş, A. M. (2023). Determination of the appropriate zone on dam surface for floating photovoltaic system installation using RS and GISc technologies. International Journal of Engineering and Geosciences, 8(1), 63-75

producing electricity from solar insolation are the most prominent. The conversion from solar to electrical energy is made by photovoltaic (PV) cells, which have been used since the 1950s. PV-SPPs comprise many solar panels, and the total radiation coming to the surface of the panels directly affects the efficiency of the system [9]. The direct solar radiation and the absence of shadows on the module surfaces provide maximum efficiency in PV-SPPs throughout the year. Shading in SPPs installed on building roofs or facades is generally high due to environmental factors. It is desirable to place the panels in the most appropriate position and angle to reduce the shading effect in collecting solar insolation [10].

SPPs can be installed on marginal agricultural lands [11], roofs [12, 13] or hydrographic surfaces, such as seas, lakes, dams, and canals [14, 15]. In floating PV (FPV) plants installed on the water surface, the environmental impact causing shading is reduced, and more solar radiation is used. Moreover, FPV-SPPs generate more energy than terrestrial systems, as they reduce the panel temperature of water [16]. The panels that cover the water surface also reduce the amount of evaporation, prevent sunlight from penetrating deep, reduce algae growth, and keep the water clean [17]. Particularly, FPV-SPPs aiming to make idle water surfaces usable for energy production are used in several countries, such as the US, Australia, Japan, China, South Korea, Brazil, and India [18].

Hydroelectric power plants (HPPs) are one of the most suitable surfaces for FPV-SPP installation due to the existing electrical energy infrastructure. However, the dynamic water level of dams can cause radical changes in shoreline boundaries. In this case, the FPV plant, which is planned to float continuously, may go aground and its electrical efficiency may decrease. Also, sharp rocks below the water level in the reservoir may rise to the surface with the withdrawal of water and damage the panels. To prevent these problems, the plant's design

should be made by considering in advance the possible changes in the dam boundaries [19]. These changes can be determined from evaluations made from the past to the present.

Energy efficiency for FPV-SPPs installed on water surfaces is usually calculated by ignoring the shading effect [20]. However, the topography of the land around the dam and other artificial elements in the area can create a shading effect on the water surface throughout the day. Various software developed to process geographical data includes analysis tools that gauge the amount of shading in a region during the day. For instance, hillshade analysis tools of geographical information system (GIS) software can be used to determine the shading effect. Solar analysis tools that consider the shading effect can be used to calculate solar radiation values for a given geographical location in certain periods [21]. Topographical factors such as differences in elevation and slope changes that make up the terrestrial shapes in the region are the main factors used in calculating the amount of shading and solar radiation [22].

RS and geographical information science (GISc) technologies include highly effective tools for monitoring water dynamics and changes in surface boundaries, shading, and solar radiation analysis from past to present [5]. In this study, the minimum limits due to the reduction in dam waters were determined by supervised classification using Landsat-5 Thematic Mapper (TM), Top of Atmosphere (TOA), Landsat-8 Operational Land Imager (OLI), and Sentinel-2 Multi-Spectral Instrument (MSI) L2A satellite images. The small islets formed from sharp rocks, which prevent the installation of FPV-SPP on the water surface, have emerged with the withdrawal of the dam water. These islets, whose positions and geometric shapes cannot be easily detected with traditional terrestrial surveying methods, can be easily detected by RS from the classified images. The water dynamics in this study area were extracted from the dataset created by Pekel et al. [6] using 32-year Landsat images. The calculated dam boundaries and water dynamics relationships were then compared. Later, an annual solar radiation map was created using the ArcGIS solar analysis tool. The area on the dam water surface in the prepared annual insolation map is classified according to solar energy potential. This study revealed the importance of RS and GISc opportunities in the facility of FPV-SPPs.

1.1. Literature Review

Water dynamics and surface boundary changes can be determined by pixel-based classification techniques using Landsat and Sentinel images [23]. There is various commercial software, such as ENVI, ERDAS, and eCognition, that can run supervised and unsupervised classification algorithms. Also, Google Earth Engine (GEE) platform, which can process big data and work in the cloud, is frequently used in pixel-based classification studies.

It is possible to determine the changes in large water masses up to 40 years with RS. However, computer systems with a powerful CPU and enough storage space are required to download and process many satellite images taken periodically. The long-term analyses conducted contribute to additional costs in the project budgets [24]. To eliminate this disadvantage today, Google has developed the GEE platform to map large areas of human settlements, analyse past changes and constantly update current estimates [25]. Operating in a cloud environment, GEE can simultaneously and easily access all the archives of Landsat and Sentinel images [26]. The GEE application interface allows development with JavaScript and Python scripting languages to access and analyse petabytes of data [27]. GEE is an effective platform for determining water dynamics, investigating temporal changes in water bodies, and monitoring seasonal changes [28]. Pekel et al. [6] analysed 32 years of water dynamics between 1984 and 2015, using more than three million Landsat images on a world scale with GEE. Chen et al. [29], Wang et al. [30], Xia et al. [31], and Deng et al. [32] have used GEE for making lake maps in China, determining maximum and minimum water coverage, and monitoring water surface changes. Nguyen et al. [33] performed a fully automated water surface extraction for New Zealand using Automated Water Extracting Index derived from Landsat-8 OLI images on the GEE platform. Jena et al. [34] and Bi et al.

[35] used the GEE platform to detect the seasonal variation of water surfaces.

It is vital to determine the appropriate locations where panels can be placed for FPV-SPPs to be installed on the water surface. Surface boundaries should be monitored in the long term for SPPs to be established, especially in dams, where water dynamics change rapidly [19]. Today, FPV systems are used less often than terrestrial PV systems. For this reason, an adequate academic examination of the issues facing the use of the FPV-SPP plant has not been established. There are quite a few studies where shading analysis is performed on the surfaces where they are installed due to the shading effect of PV systems to be installed on terrestrial surfaces [13]. For systems to be installed on marginal agricultural lands, many criteria, such as proximity to the road and transformer centre, land use, and topographic features, are considered. Approaches such as Multiple-Criteria Decision-Making [36] Analytic Hierarchy Process [37] and Artificial Neural Networks [38] are used to determine the effects of these criteria. Enough work has not been done to investigate the effect of shading on water surfaces in the installation of FPV systems. Song and Choi [20] performed a shading analysis using a digital elevation model with a fish-eye lens camera in a mine lake in Korea. Sahu et al. [39] suggested using RS and GIS-based techniques to increase the efficiency potential of FPV projects. Kumar [40] aimed to find the solar energy potential for the southern part of India through the application of different solar radiation, geology, topography, atmospheric conditions, slope, and geospatial technology. Abid et al. [15] In the 2MW FPV system in India, the shading of artificial elements around the lake was considered. However, determining the water surface boundaries where an FPV-SPP will be established and locating the facility in the region where the highest efficiency will be obtained is vital for researchers and investors.

2. Method

2.1. Study Area

This study was conducted in the Demirköprü Dam, which is in Manisa Province in the southwest of Turkey, which was put into operation for irrigation, flood control, and energy production in 1960 (Fig. 1). Demirköprü Dam is fed by the Demirci Stream from the north, Gediz River and Deliniş Stream from the East. The topography around the dam is in a wavy form, and this region is covered by oak forests, farmlands and bare lands. The area and water volume of the dam, which is the earth's body fill type, are 3,000 ha and 4,300,000 m^3, respectively [41]. The irrigation of 99,220 ha of agricultural land in the region is carried out from the Demirköprü Dam. A Hydro-electric Power Plant (HPP) with a 69 MW generating 193 GWh of electrical energy annually has been installed on the dam. The dam boundaries and water volume often vary depending on irrigation uses, electricity generation, and seasonal transitions. Agricultural irrigation activities are performed annually in the region from the beginning of August to the end of October. Concurrently, the amount of evaporation increased due to hot climatic conditions in the region between July and November. During this period, the water level usually dropped below average.

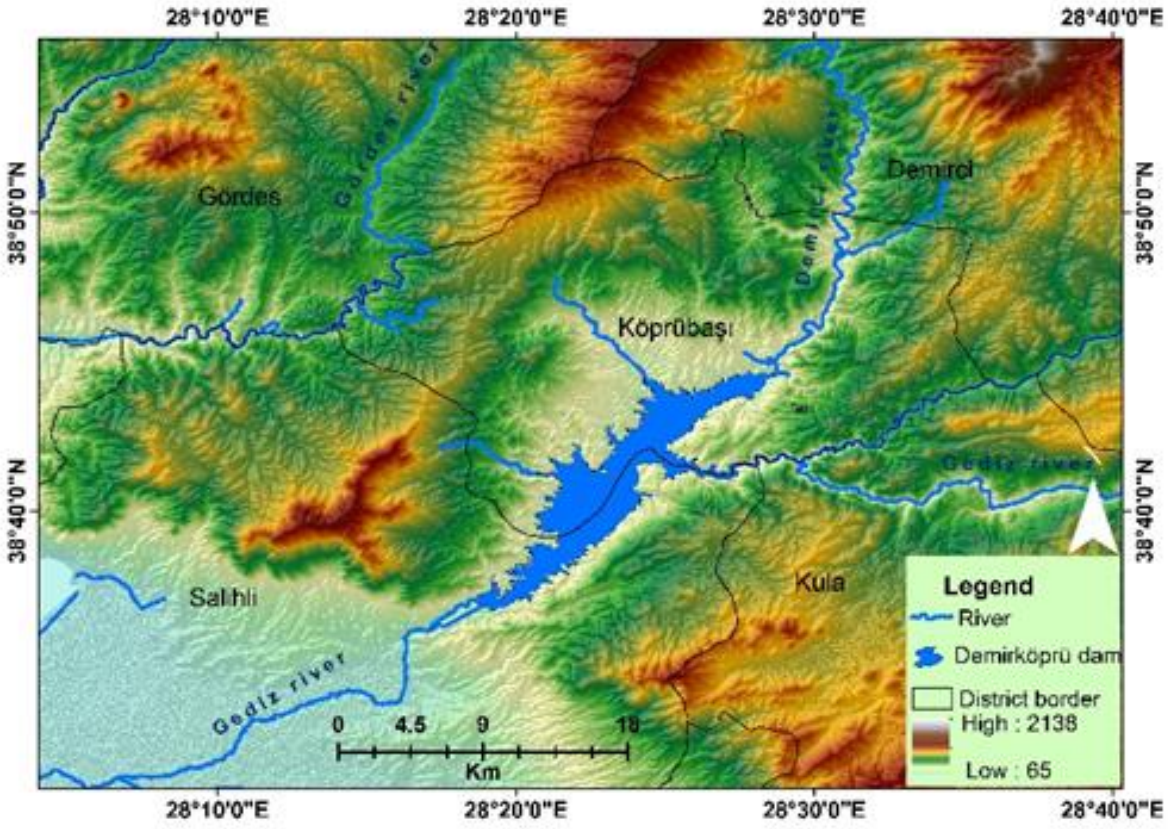

Figure 1. Location of the study area: Demirköprü Dam

2.2. Process steps in the article

In this study, changes in water surface boundaries and annual total solar insolation values were calculated based on the amount of shading on the water surface. These changes were then classified to determine the appropriate regions for the FPV-SPPs to be installed on the surface of the Demirköprü Dam. Changes in dam boundaries have been studied using two different methods. First, based on classification processes performed on images taken from satellite platforms. Second, the water surface changes in the dam area were monitored based on the surface water dynamics analysis proposed by Pekel et al. [6]. The analysis study was conducted using 3,066,080 images obtained from Landsat - 5 (TM), Landsat - 7 (ETM +), and Landsat - 8 (OLI) satellites covering the years 1984–2015. Landsat images have a temporal resolution of 16 days and a spatial resolution of 30 m. The constellation Sentinel-2A and Sentinel-2B together have a temporal resolution of 5 days. Sentinel satellite images provide data with 13 spectral bands, 12-bit radiometric resolution, and spatial resolution between 10-60 m.

The minimum limit for the installation of FPV-SPPs was determined by evaluating the information regarding the shoreline changes obtained from these two methods. Later, a solar insolation map was created considering the shading on the water surface within these boundaries using 30 m Shuttle Radar Topography Mission (SRTM) data covering the dam and its immediate surroundings. This insolation map is classified according to solar energy potential using the Jenks Natural Break (JNB) algorithm. The flow chart of the process steps is given in Fig. 2.

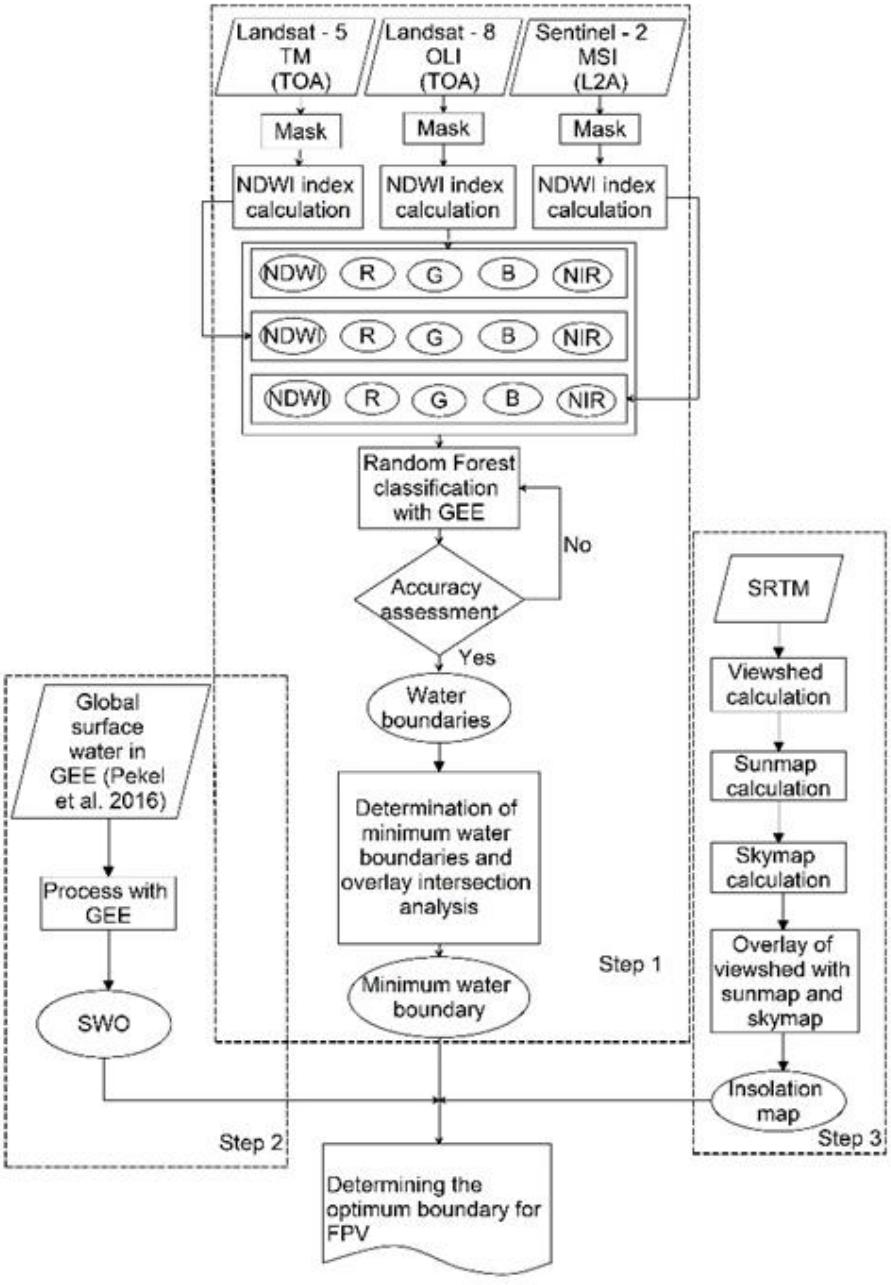

Figure 2. Flow chart of the analysis methodology

3. Results

3.1. Investigation of dam water surface change using satellite images

There are oak forests, planted agricultural areas, and bare areas around Demirköprü Dam. To detect the changes in these areas, 55 satellite images covering a span of 20 years from 1999–2019 have been classified. These images taken from Landsat-5, Landsat-8, and Sentinel-2 platforms in August, September, and October, when the dam water level was lowest, were classified by the RF algorithm in the GEE platform.

The red, green, blue, and infrared band data of each satellite image were used to distinguish the shoreline of the dam from other details. In addition to these bands, NDWI values suitable for the general characteristics of the region were calculated and included in the classification to extract the dam surface more sensitively. The accuracies of the performed classification operations were analysed by calculating producer's accuracy (PA), user's accuracy (UA), overall accuracy (OA), and kappa (K) values for each class. Among the images with an OA value over 90%, the water surface areas calculated as less than the 2,000-ha threshold are given in Table 1.

Table 1. High accuracy image classification results for Demirköprü Dam

Date	Spacecraft ID/Sensor	Area (ha)	PA (%)	UA (%)	OA (%)	K
14.08.2001	Landsat-5 (TM)	1741.6	100.0	99.9	92.0	0.882
15.09.2001		1711.5	100.0	99.9	94.8	0.924
01.10.2001		1694.7	100.0	99.9	93.1	0.899
10.09.2005		1979.6	100.0	100.0	93.1	0.899
15.08.2007		1625.2	100.0	99.8	93.1	0.898
16.09.2007		1601.8	100.0	99.7	93.2	0.901
21.08.2008		1603.2	99.7	99.8	95.1	0.928
07.09.2017	Sentinel-2 L2A (MSI)	1794.0	100.0	100.0	92.2	0.882
01.08.2018		1883.2	100.0	99.9	93.2	0.893
02.09.2018		1754.0	100.0	100.0	92.9	0.893
07.09.2019		1877.5	100.0	100.0	92.5	0.886

Among the 11 high-accuracy water surfaces derived by classification processes, five surfaces whose area values are smaller than the others are shown in Fig. 3 (a-e). The smallest surface found by the intersection of the dam surfaces derived by the classification defines the minimum boundaries of the Demirköprü Dam that constantly retains water Fig. 3 (f). This intersection area has been calculated as 1,562.4 ha [19].

On the dates when the dam's water level and surface area decrease, some small islets not visible at other times appear near the shores. Since these islets can damage FPV panels, their location and shape should be precisely established in advance. Furthermore, they can also be used as the fixing point of the panels as required. Their positions can be determined from Sentinel images with higher resolutions than Landsat images. Some of the islets determined from the classification are shown in red ellipses in Fig. 4. It is complex to determine their positions and shapes using classical terrestrial survey methods. The islets were precisely determined using high-resolution satellite images of these dates after determining that the dates of the dam water level were low.

3.2. Water dynamics for the Demirköprü Dam

Global surface water dynamics have been analysed by classifying spatial detail and accuracy levels at intervals of 5–10 years using medium-resolution Landsat satellite images covering 32 years [6]. In this study, NDWI was used to separate water from other details, and Hue-Saturation-Value (HSV) colour-space was used for image enhancement. Thematic maps were produced to characterize the water transitions between the first observation year and the last observation year. In the thematic maps produced, they stated that there was no significant change in the water in the black areas between 1984 and 2015, that the water increased in the green areas and decreased in the red areas. In addition, they divided the passages of water into different categories in their study. These categories are permanent water surfaces, new permanent water surfaces, lost permanent water surfaces, seasonal water surfaces, new seasonal water surfaces, lost seasonal water surfaces, conversion of permanent water into seasonal water.

Spectral library equations defining the classes used in the study were created through visual analysis. The performance of the global classification processes has been evaluated using 40,124 control points, and it has been proven that the accuracy is around 99% in the calculation. The derived global dataset has facilitated modelling of the water surface, mapping long-term changes in global water formation, tracking changes in freshwater resources, such as lakes and rivers, and tracking climatic changes.

During the monitoring period, the surface areas where water resources, such as waterbeds, rivers, dams, and lakes, remain constant have been determined. The permanent state of surface water is presented based on a single map called Surface Water Occurrence (SWO). Monthly SWO data were calculated using Eq.1 [6].

$$SWO^{month} = \sum WD^{month} / \sum VO^{month} \quad (1)$$

Where, WD is the monthly amount of water detected and VO is the number of valid observations.

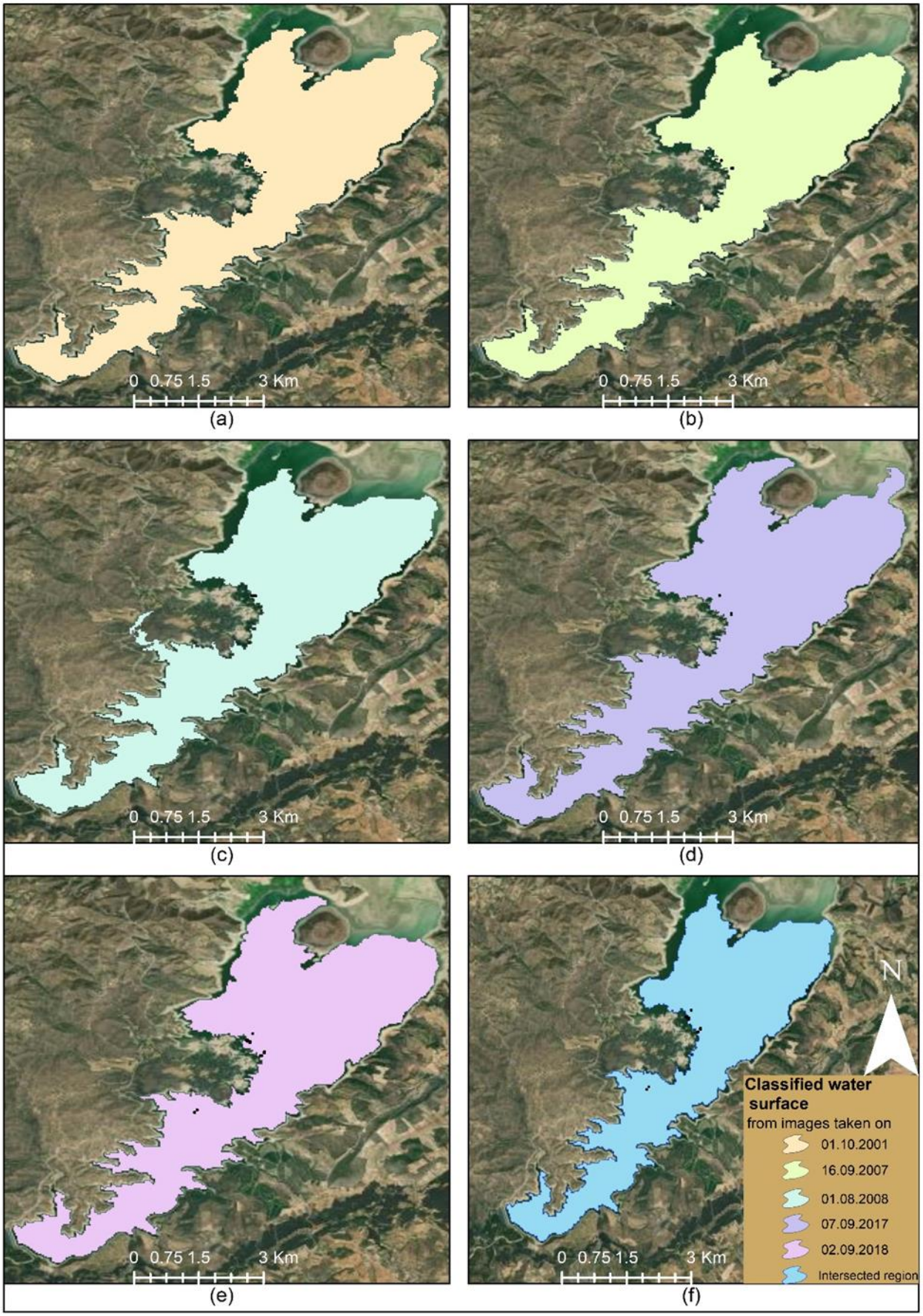

Figure 3. Five classifications with the smallest surface area (a–e) and the intersection of the surfaces (f)

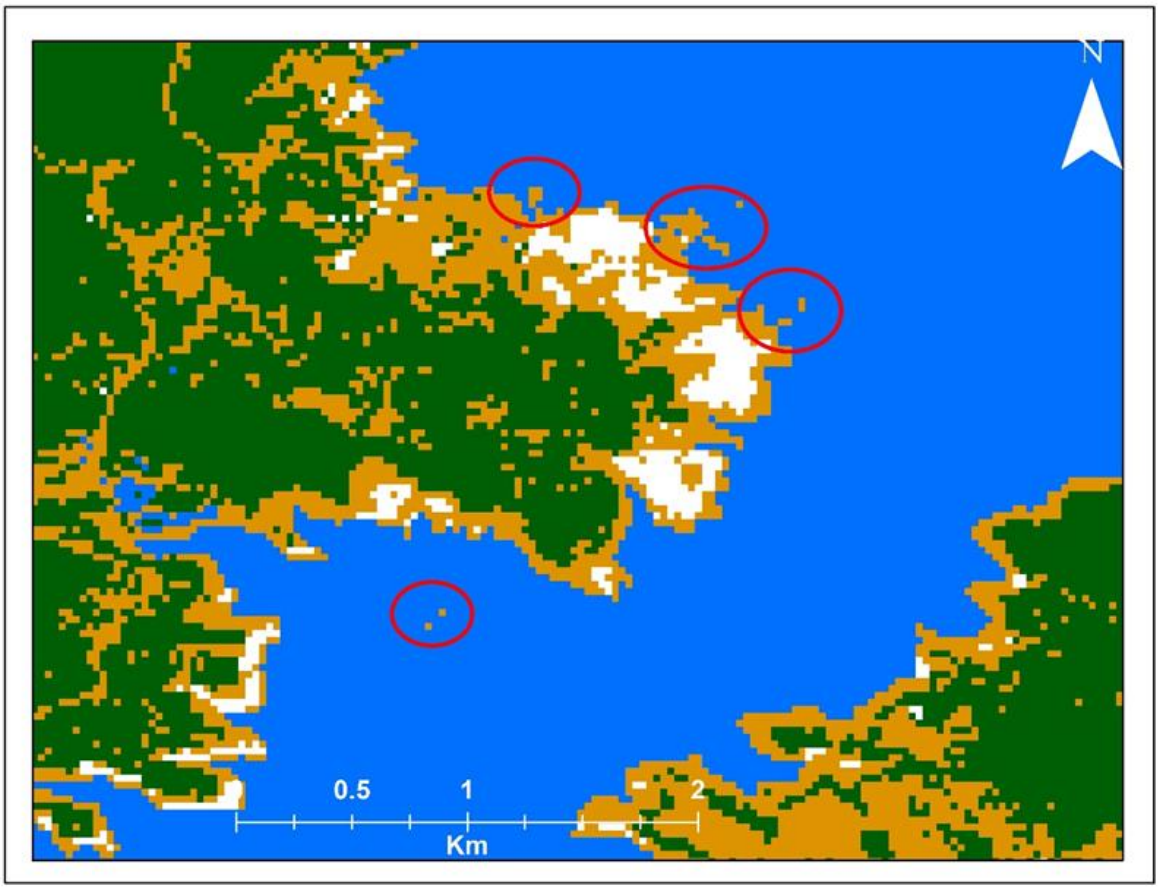

Figure 4. Islets extracted with the Sentinel 2A image dated 02.09.2018 are marked with red ellipses

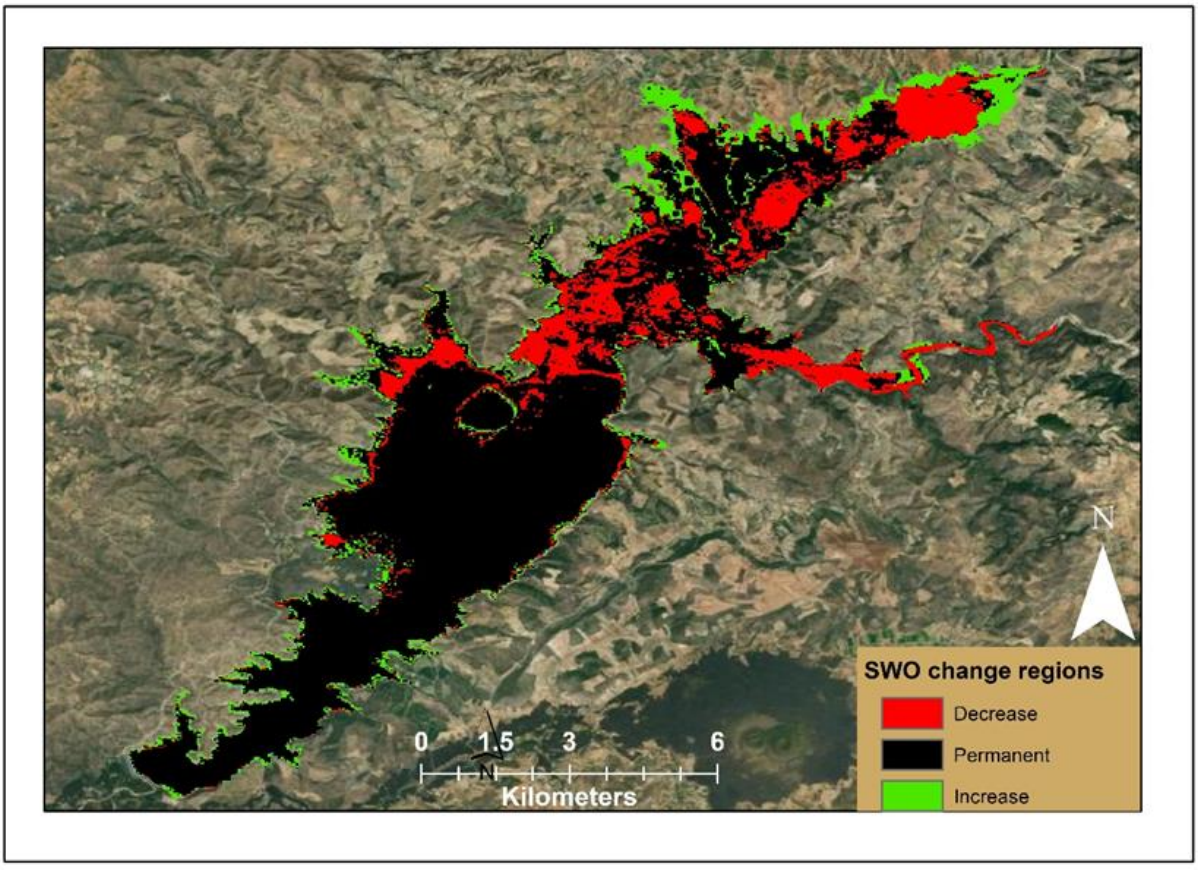

Fig. 2 SWO change map between 1984–2015 for Demirköprü Dam

This study, which is very useful in terms of interpreting the analyses and validating the methods used and carried out by writing code on the GEE platform, can be used as a ready data set in many academic studies.

32 years of global water dynamics analysis provides a map explaining the water dynamics in Demirköprü Dam. The change in the dam is in the form of continuous advancement and withdrawal of the shoreline. Increases in water formation are represented in green and decrease in red on the SWO map (Fig. 5). The regions with permanent water and no significant change in water formation between 1984 and 2015 are shown in black.

The region from the south to the middle of the dam is where water is constantly available. Time-dependent increases are observed in the coastal areas of this region. In contrast, the water is more dynamic in the northern part of the dam. Demirci Stream feeding from the north, Deliniş Stream, and Gediz River feeding on the east make Demirköprü Dam dynamic. Depending on the topographical formation, the transitivity that triggers the increases and decreases in the water level in the northern region is revealed by the SWO map. The currents formed in the northern part of the dam indicate that this area is unsuitable for FPV SPP installation.

The coherence between the SWO map and the Demirköprü Dam surface map obtained by the classification method was examined with the Kappa statistical test using randomly selected 1,000 points (Table 2). Kappa value calculated between the SWO map and the dam surface maps derived from the images dated September 2005, August 2018, and September 2019 are over 0.8. Kappa values higher than the threshold value indicate a very high agreement between the SWO map and the classified maps [42]. The areas with a Kappa value of less than 0.8 were found to be relatively lower than those in the fields on other dates. In this case, it was determined that the compatibility of these maps with the SWO map was lower, so according to the SWO map, the water level at those dates decreased more than the usual situation.

Consequently, in the last two decades, it has been determined that the withdrawal of water in Demirköprü Dam was high in August 2001, September 2001, October 2001, August 2007, September 2007, August 2008, September 2017, and September 2018.

Table 2. Accuracy test of the SWO map with images of the lowest water surface area maps

SWO change map	Date	Spacecraft ID/Sensor	K
Permanent data	14.08.2001	Landsat-5 (TM)	0.792
	15.09.2001		0.790
	01.10.2001		0.782
	10.09.2005		0.828
	15.08.2007		0.744
	16.09.2007		0.732
	01.08.2008		0.708
	07.09.2017	Sentinel-2 L2A (MSI)	0.790
	01.08.2018		0.808
	02.09.2018		0.770
	07.09.2019		0.810

3.3. Insolation map

The efficiency of PV systems depends on the amount of incident solar radiation on the panels' surfaces [43]. Topographical factors such as elevation, aspect, and slope affect the amount of incident solar radiation on the panel surface (Fig. 6). The spatial and temporal variations of this amount are revealed by solar radiation modeling. Modeling shows the effects of the sun on a geographical area for certain periods by spatial analysis based on topographic data [44]. Today, it is possible to produce solar radiation maps for a region using the solar analysis tools provided by GISc over the digital elevation model (DEM) dataset [45].

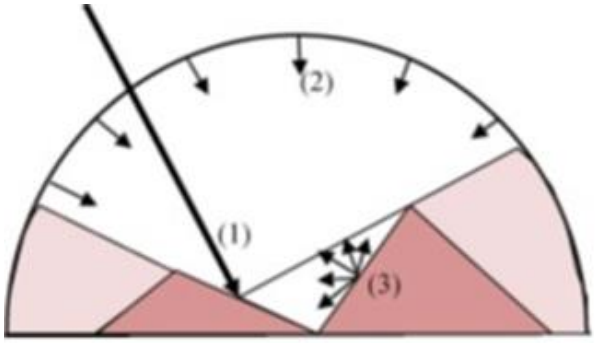

Figure 6. Solar energy sources on a surface: (1) direct radiation, (2) diffuse radiation reflected from the sky, and (3) diffuse radiation reflected from land [21]

In this study, solar radiation maps were created using the ArcGIS/Area Solar Radiation tool of ESRI, which offered comprehensive geometric modeling, high calculation speed, and accuracy [46]. A 30 m spatial resolution SRTM dataset was used to regionally map the amount of solar radiation that varies depending on the land topography and sun incidence angles. The annual total radiation of 2020 was calculated for each pixel in the area that includes Demirköprü Dam (Fig. 7). In the annual radiation calculation, the general parameters used according to the latitude of the region and the calculation period were selected as day interval 14, hour interval 0.5, and SkySize 200 [47]. Topographic and radiation parameters are given in Table 3.

Annual insolation map with 30 m spatial resolution for Demirköprü Dam and its near surroundings using SRTM DEM data overlaps with the smallest dam area given in Fig. 3 (f) and given in Fig. 5 (a). Solar radiation values calculated within the intersection field vary between 1,554 kWh/m^2-year and 1,875 kWh/m^2-year. This change is due to the shading caused by the topography around the dam. To reveal the effect of shading on the intersection region, 30 m resolution pixels were reclassified using the JNB algorithm according to the insolation value Fig. 7 (b). The classification made into five categories showed that insolation in the regions close to the shoreline of the dam was lower than in the inner regions (Table 4).

Table 3. Solar radiation parameters used in this study

Topographic parameters			Radiation parameters				
Z factor	Calculation directions	Calculation direction	Zenith divisions	Azimuth divisions	Diffuse model type	Diffuse Proportion	Transitivity
1	DEM	16	8	8	Standard overcast sky	0.5	0.5

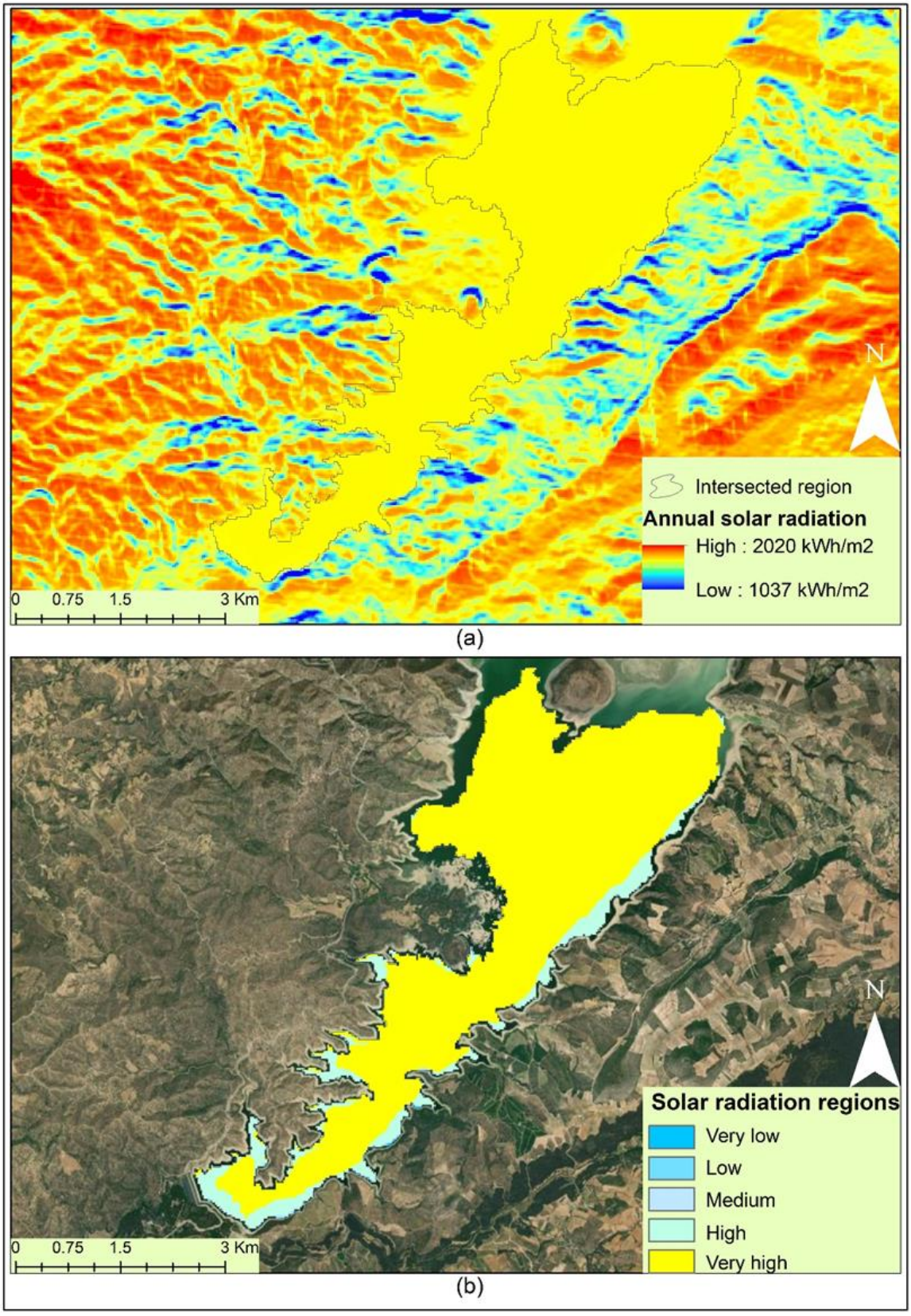

Figure 3. a) Annual insolation map of Demirköprü Dam and its near surround, b) classified solar radiations in the dam surface

Table 4. Classes calculated according to the JNB algorithm

Solar radiation value (kWh/m²)	Category	Area (ha)	Percentage (%)
1,796.8-1,875.2	Very High	1383.1	88.5
1,782.1-1,796.8	High	169.8	10.9
1,729.3-1,782.0	Medium	7.3	0.5
1,648.6-1,729.0	Low	1.4	0.1
1,554.0-1,648.6	Very Low	0.8	0.1

The area with very high insolation covers 88.5% of the dam area. Regions with medium, low, and very low insolation amounts constitute 0.6% of the total dam area. The insolation values of the regions on the shoreline in the east, south, and west of the dam basin are due to the wavy structure of the dam's shoreline and sharp rocks. The 10.9% of parts of the dam, which is a little further from the shoreline, is classified as high regarding insolation. Although this region is classified as high, it appears that there is some shading effect. When investing in FPV systems, it is important to valorise the shadowing effect in this region.

4. Discussion

The application of PV systems to water surfaces is a new and rapidly developing application in the world. A limited number of studies have been found on investigating the shading effect on water surfaces. For the installation of FPV systems, it is very important to calculate the water surface boundaries with the least error and to choose the most suitable places for installation. In the literature review, it is seen that RS and GIS techniques are widely used in determining the appropriate location of FPV systems. Especially in water surface applications, Sahu et al. [39] suggested the use of RS and GIS techniques in terms of increasing efficiency. In this study, the 20-year change in the area was examined by using RS to determine the suitable area for the FPV-GES installation on the Demirköprü dam water surface and was confirmed by the study by Pekel et al. [6].

The most important factor in the generation of electrical energy of photovoltaic systems is the amount of radiation falling on the module surface. Shading of the solar radiation of some module surfaces in the array due to any environmental factor affects the module efficiency, array efficiency and thus the efficiency of the PV system [48–52]. Various techniques are applied to reduce the shading effect [53]. However, applying strategies such as electrical interconnection changes or using microinverters in large-scale systems makes the system complex and increases its cost. The most practical and economical method to minimize the effect of shading is to determine the no shading or least shading areas. The ArcGIS solar radiation tool is frequently used to detect the total radiation in an area along with the effect of topography [54–58].

When the studies on FPV systems were examined, Kim et al. [59] focused on the selection of suitable sites. In their study, they created a water depth database using OpenAPI and estimated the radiation distribution using meteorological and topographical data. While the depth of the water was taken into account in that study, in our study, the surface area of the water, and therefore the horizontal shoreline change, was taken into account, since it was aimed to use the entire surface. In addition, the importance of topography in radiation distribution has been revealed. Lee and Lee [60] identified suitable locations for FPV systems with the Analytical Hierarchy Process (AHP) considering terrain and climatic factors. In their study, suitable river surface areas for FPV installation were determined using GIS techniques, while in this study, suitable areas of the dam surface were determined. Both studies are similar in this aspect.

5. Conclusion

The minimum areas in the classifications made using the RF Algorithm and NDWI over the Landsat and Sentinel satellite images of the Demirköprü Dam for the last 20 years were analyses with the GIS overlay tool, and the optimum area was calculated as 1,562.4 ha. Since the investment costs of FPVs are high, it is vital to precisely establish the water surfaces. Also, it was concluded that the detection of small islands caused by the decrease of the water level by remote sensing will be important in the net detection and fixation of the installation areas of FPV systems. According to this result, the regions with islets can only be used for fixation purposes.

Pekel et al. [6], a global water-formation study conducted on a world scale was applied for Demirköprü dam and the results were consistent with the determined dam boundaries. It has been realized that both approaches can be used as alternatives to each other in monitoring changes on the dam surface.

Shading on the surfaces of PV panels reduces their efficiency. Classification of annual solar analysis results for the dam surface is invaluable in determining the regions where maximum energy efficiency can be achieved. Although the total radiation is high in the middle parts of the reservoir, the total amount of radiation falling on the surface decreases in the regions close to the shoreline due to the effect of the shading caused by the topography. This will cause a decrease in the amount of electrical energy to be generated from the FPV panels installed in regions close to the shoreline of the reservoir. As a result, this study revealed the importance of using RS and GISc technologies in determining the optimum region for FPV power plants to be installed on dam water surfaces.

Acknowledgement

This research did not receive any specific grant from funding agencies in the public, commercial, or not-for-profit sectors and it was prepared from a part of the first author's doctoral dissertation.

Author contributions

Osman Salih Yılmaz: Conceptualization, Methodology, Software, Field study **Fatih Gülgen:** Data curation, Writing-Original draft preparation, Software, Validation., Field study **Ali Murat Ateş:** Visualization, Investigation, Writing-Reviewing and Editing.

Conflicts of interest

The authors declare no conflicts of interest.

References

1. Du, Z., Bin, L., Ling, F., Li, W., Tian, W., Wang, H., ... & Zhang, X. (2012). Estimating surface water area changes using time-series Landsat data in the Qingjiang River Basin, China. *Journal of Applied Remote Sensing*, *6*(1), 063609. https://doi.org/10.1117/1.jrs.6.063609
2. Molden, D. J., Vaidya, R. A., Shrestha, A. B., Rasul, G., & Shrestha, M. S. (2014). Water infrastructure for the Hindu Kush Himalayas. *International Journal of Water Resources Development*, *30*(1), 60-77.
3. Du, Y., Zhang, Y., Ling, F., Wang, Q., Li, W., & Li, X. (2016). Water bodies' mapping from Sentinel-2 imagery with modified normalized difference water index at 10-m spatial resolution produced by sharpening the SWIR band. *Remote Sensing*, *8*(4), 354. https://doi.org/10.3390/rs8040354
4. Yang, X., & Chen, L. (2017). Evaluation of automated urban surface water extraction from Sentinel-2A imagery using different water indices. *Journal of Applied Remote Sensing*, *11*(2), 026016.. https://doi.org/10.1117/1.JRS.11.026016
5. Su, H., Peng, Y., Xu, C., Feng, A., & Liu, T. (2021). Using improved DeepLabv3+ network integrated with normalized difference water index to extract water bodies in Sentinel-2A urban remote sensing images. *Journal of Applied Remote Sensing*, *15*(1), 018504.
6. Pekel, J. F., Cottam, A., Gorelick, N., & Belward, A. S. (2016). High-resolution mapping of global surface water and its long-term changes. *Nature*, *540*(7633), 418-422. https://doi.org/10.1038/nature20584
7. Arekhi, M., Goksel, C., Balik Sanli, F., & Senel, G. (2019). Comparative evaluation of the spectral and spatial consistency of Sentinel-2 and Landsat-8 OLI data for Igneada longos forest. *ISPRS International Journal of Geo-Information*, *8*(2), 56. https://doi.org/10.3390/ijgi8020056
8. Dehwah, A. H., Asif, M., & Rahman, M. T. (2018). Prospects of PV application in unregulated building rooftops in developing countries: A perspective from Saudi Arabia. *Energy and Buildings*, *171*, 76-87. https://doi.org/10.1016/j.enbuild.2018.04.001
9. Singh, A. K., Boruah, D., Sehgal, L., & Ramaswamy, A. P. (2019). Feasibility study of a grid-tied 2MW floating solar PV power station and e-transportation facility using 'SketchUp Pro'for the proposed smart city of Pondicherry in India. *Journal of Smart Cities*, *2*(2), 49-59. https://doi.org/10.18063/jsc.2016.02.004
10. García-Pérez, S., Sierra-Pérez, J., & Boschmonart-Rives, J. (2018). Environmental assessment at the urban level combining LCA-GIS methodologies: A case study of energy retrofits in the Barcelona metropolitan area. *Building and Environment*, *134*, 191-204. https://doi.org/10.1016/j.buildenv.2018.01.041
11. Merrouni, A. A., Elalaoui, F. E., Mezrhab, A., Mezrhab, A., & Ghennioui, A. (2018). Large scale PV sites selection by combining GIS and Analytical Hierarchy Process. Case study: Eastern Morocco. *Renewable energy*, *119*, 863-873.
12. Yilmaz, S., Ozcalik, H. R., & Dincer, F. (2015). Remote detection and assessment of solar energy potential analysis based on available roof surface area: case study in Kahramanmaras, Turkey. *Journal of Applied Remote Sensing*, *9*(1), 097698. https://doi.org/10.1117/1.jrs.9.097698
13. Gagnon, P., Margolis, R., Melius, J., Phillips, C., & Elmore, R. (2018). Estimating rooftop solar technical potential across the US using a combination of GIS-based methods, lidar data, and statistical modeling. Environmental Research Letters, 13, 1748–9326. https://doi.org/10.1088/1748-9326/aaa554
14. Czirjak, D. W. (2017). Detecting photovoltaic solar panels using hyperspectral imagery and estimating solar power production. *Journal of Applied Remote Sensing*, *11*(2), 026007. https://doi.org/10.1117/1.jrs.11.026007
15. Abid, M., Abid, Z., Sagin, J., Murtaza, R., Sarbassov, D., & Shabbir, M. (2019). Prospects of floating photovoltaic technology and its implementation in Central and South Asian Countries. *International Journal of Environmental Science and Technology*, *16*(3), 1755-1762. https://doi.org/10.1007/s13762-018-2080-5
16. Pimentel Da Silva, G. D., & Branco, D. A. C. (2018). Is floating photovoltaic better than conventional photovoltaic? Assessing environmental impacts. *Impact Assessment and Project Appraisal*, *36*(5), 390-400. https://doi.org/10.1080/14615517.2018.1477498
17. Mansouri Kouhestani, F., Byrne, J., Johnson, D., Spencer, L., Hazendonk, P., & Brown, B. (2019). Evaluating solar energy technical and economic potential on rooftops in an urban setting: the city of Lethbridge, Canada. *International Journal of Energy and Environmental Engineering*, *10*(1), 13-32. https://doi.org/10.1007/s40095-018-0289-1
18. Ranjbaran, P., Yousefi, H., Gharehpetian, G. B., & Astaraei, F. R. (2019). A review on floating photovoltaic (FPV) power generation units. *Renewable and Sustainable Energy Reviews*, *110*, 332-347. https://doi.org/10.1016/j.rser.2019.05.015
19. Ates, A. M., Yilmaz, O. S., & Gulgen, F. (2020). Using remote sensing to calculate floating photovoltaic technical potential of a dam's surface. *Sustainable Energy Technologies and Assessments*, *41*, 100799. https://doi.org/10.1016/j.seta.2020.100799

20. Song, J., & Choi, Y. (2016). Analysis of the potential for use of floating photovoltaic systems on mine pit lakes: case study at the ssangyong open-pit limestone mine in Korea. *Energies*, *9*(2), 102.
21. Charabi, Y., & Gastli, A. (2010). GIS assessment of large CSP plant in Duqum, Oman. *Renewable and Sustainable Energy Reviews*, *14*(2), 835-841.
22. Dubayah, R., & Rich, P. M. (1995). Topographic solar radiation models for GIS. *International journal of geographical information systems*, *9*(4), 405-419.
23. Zhang, Y., Gao, J., & Wang, J. (2007). Detailed mapping of a salt farm from Landsat TM imagery using neural network and maximum likelihood classifiers: a comparison. *International Journal of Remote Sensing*, *28*(10), 2077-2089. https://doi.org/10.1080/01431160500406870
24. Zurqani, H. A., Post, C. J., Mikhailova, E. A., & Allen, J. S. (2019). Mapping urbanization trends in a forested landscape using Google Earth Engine. *Remote Sensing in Earth Systems Sciences*, *2*(4), 173-182.
25. Patel, N. N., Angiuli, E., Gamba, P., Gaughan, A., Lisini, G., Stevens, F. R., ... & Trianni, G. (2015). Multitemporal settlement and population mapping from Landsat using Google Earth Engine. *International Journal of Applied Earth Observation and Geoinformation*, *35*, 199-208. https://doi.org/10.1016/j.jag.2014.09.005
26. Xiong, J., Thenkabail, P. S., Gumma, M. K., Teluguntla, P., Poehnelt, J., Congalton, R. G., ... & Thau, D. (2017). Automated cropland mapping of continental Africa using Google Earth Engine cloud computing. *ISPRS Journal of Photogrammetry and Remote Sensing*, *126*, 225-244. https://doi.org/10.1016/j.isprsjprs.2017.01.019
27. Dong, J., Xiao, X., Menarguez, M. A., Zhang, G., Qin, Y., Thau, D., ... & Moore III, B. (2016). Mapping paddy rice planting area in northeastern Asia with Landsat 8 images, phenology-based algorithm and Google Earth Engine. *Remote sensing of environment*, *185*, 142-154. https://doi.org/10.1016/j.rse.2016.02.016
28. Pekel, J. F., Cottam, A., Clerici, M., Belward, A., Dubois, G., Bartholome, E., & Gorelick, N. (2014, December). A Global Scale 30m Water Surface Detection Optimized and Validated for Landsat 8. In *AGU Fall Meeting Abstracts* (Vol. 2014, pp. H33P-01).
29. Chen, B., Xiao, X., Li, X., Pan, L., Doughty, R., Ma, J., ... & Giri, C. (2017). A mangrove forest map of China in 2015: Analysis of time series Landsat 7/8 and Sentinel-1A imagery in Google Earth Engine cloud computing platform. *ISPRS Journal of Photogrammetry and Remote Sensing*, *131*, 104-120. https://doi.org/10.1016/j.isprsjprs.2017.07.011
30. Wang, C., Jia, M., Chen, N., & Wang, W. (2018). Long-term surface water dynamics analysis based on Landsat imagery and the Google Earth Engine platform: A case study in the middle Yangtze River Basin. *Remote Sensing*, *10*(10), 1635. https://doi.org/10.3390/rs10101635
31. Xia, H., Zhao, J., Qin, Y., Yang, J., Cui, Y., Song, H., ... & Meng, Q. (2019). Changes in water surface area during 1989–2017 in the Huai River Basin using Landsat data and Google earth engine. *Remote Sensing*, *11*(15), 1824.
32. Deng, Y., Jiang, W., Tang, Z., Ling, Z., & Wu, Z. (2019). Long-term changes of open-surface water bodies in the Yangtze River basin based on the Google Earth Engine cloud platform. *Remote Sensing*, *11*(19), 2213. https://doi.org/10.3390/rs11192213
33. Nguyen, U. N., Pham, L. T., & Dang, T. D. (2019). An automatic water detection approach using Landsat 8 OLI and Google Earth Engine cloud computing to map lakes and reservoirs in New Zealand. *Environmental monitoring and assessment*, *191*(4), 1-12. https://doi.org/10.1007/s10661-019-7355-x
34. Jena, R., Pradhan, B., & Jung, H. (2020). Seasonal water change assessment at Mahanadi River, India using multi-temporal data in Google earth engine. Korean Journal of Remote Sensing, 36, 1–13
35. Bi, L., Fu, B. L., Lou, P. Q., & Tang, T. Y. (2020). Delineation water of pearl river basin using Landsat images from Google Earth Engine. *The International Archives of Photogrammetry, Remote Sensing and Spatial Information Sciences*, *42*, 5-10. https://doi.org/10.5194/isprs-archives-XLII-3-W10-5-2020
36. Pohekar, S. D., & Ramachandran, M. (2004). Application of multi-criteria decision making to sustainable energy planning—A review. *Renewable and sustainable energy reviews*, *8*(4), 365-381.
37. Palmas, C., Abis, E., von Haaren, C., & Lovett, A. (2012). Renewables in residential development: an integrated GIS-based multicriteria approach for decentralized micro-renewable energy production in new settlement development: a case study of the eastern metropolitan area of Cagliari, Sardinia, Italy. *Energy, Sustainability and Society*, *2*(1), 1-15. https://doi.org/10.1186/2192-0567-2-10
38. Yadav, A. K., & Chandel, S. S. (2014). Solar radiation prediction using Artificial Neural Network techniques: A review. *Renewable and sustainable energy reviews*, *33*, 772-781.
39. Sahu, A., Yadav, N., & Sudhakar, K. (2016). Floating photovoltaic power plant: A review. *Renewable and sustainable energy reviews*, *66*, 815-824. https://doi.org/10.1016/j.rser.2016.08.051
40. Kumar, D. (2019). Mapping solar energy potential of southern India through geospatial technology. *Geocarto International*, *34*(13), 1477-1495. https://doi.org/10.1080/10106049.2018.1494759
41. Kokpinar, M. A., Kumcu, S. Y., Altan-Sakarya, A., & Gogus, M. (2010). Reservoir sedimentation in the Demirköprü Dam, Turkey. *River Flow*, 1125-1130.
42. Landis, J. R., & Koch, G. G. (1977). An application of hierarchical kappa-type statistics in the assessment of majority agreement among multiple observers. *Biometrics*, 363-374.
43. Duffie, J.A., & Beckman, W. A. (2013). Solar engineering of thermal processes. John Wiley & Sons
44. Kumar, D. (2020). Satellite-based solar energy potential analysis for southern states of India. *Energy Reports*, *6*, 1487-1500.

45. Wate, P., & Saran, S. (2015). Implementation of CityGML energy application domain extension (ADE) for integration of urban solar potential indicators using object-oriented modelling approach. *Geocarto International*, *30*(10), 1144-1162. https://doi.org/10.1080/10106049.2015.1034192
46. Falklev, E. H. (2017). *Mapping of solar energy potential on Tromsøya using solar analyst in ArcGIS* (Master's thesis, UiT The Arctic University of Norway).
47. Fu, P., & Rich, P. M. (1999, July). Design and implementation of the Solar Analyst: an ArcView extension for modeling solar radiation at landscape scales. In *Proceedings of the nineteenth annual ESRI user conference* (Vol. 1, pp. 1-31). USA: San Diego.
48. Belhachat, F., & Larbes, C. (2021). PV array reconfiguration techniques for maximum power optimization under partial shading conditions: A review. *Solar Energy*, *230*, 558-582. https://doi.org/10.1016/j.solener.2021.09.089
49. Eke, R., & Demircan, C. (2015). Shading effect on the energy rating of two identical PV systems on a building façade. *Solar Energy*, *122*, 48-57. https://doi.org/10.1016/j.solener.2015.08.022
50. Mehedi, I. M., Salam, Z., Ramli, M. Z., Chin, V. J., Bassi, H., Rawa, M. J. H., & Abdullah, M. P. (2021). Critical evaluation and review of partial shading mitigation methods for grid-connected PV system using hardware solutions: The module-level and array-level approaches. *Renewable and Sustainable Energy Reviews*, *146*, 111138. https://doi.org/10.1016/j.rser.2021.111138
51. Saiprakash, C., Mohapatra, A., Nayak, B., & Ghatak, S. R. (2021). Analysis of partial shading effect on energy output of different solar PV array configurations. *Materials Today: Proceedings*, *39*, 1905-1909. https://doi.org/10.1016/j.matpr.2020.08.307
52. Seapan, M., Hishikawa, Y., Yoshita, M., & Okajima, K. (2020). Detection of shading effect by using the current and voltage at maximum power point of crystalline silicon PV modules. *Solar Energy*, *211*, 1365-1372. https://doi.org/10.1016/j.solener.2020.10.078
53. Yang, B., Ye, H., Wang, J., Li, J., Wu, S., Li, Y., ... & Ye, H. (2021). PV arrays reconfiguration for partial shading mitigation: Recent advances, challenges and perspectives. *Energy Conversion and Management*, *247*, 114738. https://doi.org/10.1016/j.enconman.2021.114738
54. Charabi, Y., Gastli, A., & Al-Yahyai, S. (2016). Production of solar radiation bankable datasets from high-resolution solar irradiance derived with dynamical downscaling Numerical Weather prediction model. *Energy Reports*, *2*, 67-73. https://doi.org/10.1016/j.egyr.2016.05.001
55. Gassar, A. A. A., & Cha, S. H. (2021). Review of geographic information systems-based rooftop solar photovoltaic potential estimation approaches at urban scales. *Applied Energy*, *291*, 116817. https://doi.org/10.1016/j.apenergy.2021.116817
56. Kumar, D. (2021). Spatial variability analysis of the solar energy resources for future urban energy applications using Meteosat satellite-derived datasets. *Remote Sensing Applications: Society and Environment*, *22*, 100481. https://doi.org/10.1016/j.rsase.2021.100481
57. Oh, M., & Park, H. D. (2018). A new algorithm using a pyramid dataset for calculating shadowing in solar potential mapping. *Renewable Energy*, *126*, 465-474. https://doi.org/10.1016/j.renene.2018.03.068
58. Settou, B., Settou, N., Gahrar, Y., Negrou, B., Bouferrouk, A., Gouareh, A., & Mokhtara, C. (2022). Geographic information-driven two-stage optimization model for location decision of solar power plant: A case study of an Algerian municipality. *Sustainable Cities and Society*, *77*, 103567. https://doi.org/10.1016/j.scs.2021.103567
59. Kim, S. M., Oh, M., & Park, H. D. (2019). Analysis and prioritization of the floating photovoltaic system potential for reservoirs in Korea. *Applied Sciences*, *9*(3), 395. https://doi.org/doi:10.3390/app9030395
60. Lee, K. R., & Lee, W. H. (2016). Floating photovoltaic plant location analysis using GIS. *Journal of Korean Society for Geospatial Information Science*, *24*(1), 51-59.